Semnan University

Mechanics of Advanced Composite Structures

journal homepage: http://MACS.journals.semnan.ac.ir

Isogeometric Free and Forced Vibration Analyses of FG-CNTs Plates based on a Logarithmic Higher-Order Shear Deformation Theory

Hassan Mohammadi *

Department of Mechanical Engineering, Islamic Azad University, Lamerd, 7434155388, Iran

KEYWORDS

Carbon nanotubes
Free vibration
Forced vibration
Isogeometric analysis
Logarithmic higher-order shear deformation theory

ABSTRACT

This paper develops the new logarithmic higher-order shear deformation theory (LHSDT) incorporating isogeometric method for free and forced vibration analyses of functionally graded carbon nanotubes reinforced composite (FG-CNTRC) plates. In this theory, a logarithmic function is employed to approximate the distribution of shear strains along the plate thickness which satisfies the condition of zero tractions on the top and bottom surfaces of the plate. The plate is assumed to be fabricated from a mixture of carbon nanotubes (CNTs) and a polymeric matrix. The CNTs are either uniformly distributed or functionally graded (FG) along the thickness direction of the plate. The modified rule of mixture scheme is applied to estimate the effective mechanical properties of FG-CNTRC plates. The governing equations are derived from Hamilton's principle. Furthermore, the Newmark approach is utilized to predict the temporal response of FG-CNTRC plates under different transverse dynamical loadings. The applicability and efficiency of the present formulation in predicting vibrational characteristics of FG-CNTRC plates are investigated through an extensive set of numerical examples considering different configurations of the plate. It is revealed that the computed results are in excellent agreement with other solution methods extracted by the 3D model and other plate theories. Eventually, a detailed parametric study is conducted to explore the influence of related parameters on the natural frequencies and temporal response of FG-CNTRC plates.

1. Introduction

It has always been a demand in science and engineering to find novel materials with improved properties. CNTs have extraordinary mechanical, thermal, and electrical properties, and therefore, they are an appropriate candidate for use as reinforcement in a polymetric matrix [1,2]. In recent years, several research papers have been published to investigate different mechanical behaviors of carbon nanotube-reinforced composite (CNTRC) structures [3-21]. In 2009, Shen [3] combined the concepts of FG distribution and CNTRCs and introduced a new class of materials known as FG-CNTRCs.

There is a rich literature on the mechanical response of FG-CNTRC plates in bending, vibration, and buckling. Especially, the vibration problem of FG-CNTRC plate structures has been solved by many researchers during the last decade. In this regard, they have employed different analytical, semi-analytical and numerical methods based on three-dimensional (3D) elasticity theory or equivalent-single-layer (ESL) theories. Depending on whether shear and normal deformation effects are taken into account, different ESL theories are derived from the 3D elasticity theory. In the simplest ESL theory, the classical plate theory (CPT), transverse shear deformation effects are ignored [22]. The CPT provides acceptable results only for thin plate structures. The next one is the first-order shear deformation theory (FSDT) which considers constant transverse shear strains. In this theory, a shear correction factor is required in order to impose the condition of zero-tractions at the inner and outer levels. The determination of this factor is difficult since it depends on the geometry and material of the plate [23]. The FSDT generates good results for thin and

* Corresponding author. Tel.: +98-9177815893
E-mail address: hmohammadi8618@gmail.com

DOI: 10.22075/MACS.2021.23147.1334
Received 21-04-14; Received in revised form 21-06-01; Accepted 21-11-18

moderately thick plates; however, it suffers from shear locking phenomena [24]. Recently, some modifications have been devoted to this theory to eliminate the condition above [24-26]. To overcome these obstacles, higher-order shear deformation theories (HSDTs) are developed. During past decades, numerous polynomial [27-30] and nonpolynomial [31-37] functions have been used by many researchers to predict the distribution of shear strains along the plate thickness. Recently, Zhu et al. [38] proposed a new logarithmic shear shape function and studied bending, free vibration, and buckling behaviors of FG plates via the isogeometric method. They showed that the presented LHSDT could predict accurate numerical results.

Isogeometric analysis (IGA) is a relatively novel numerical approach which Hughes and his co-workers proposed in 2005 [39]. IGA can be regarded as the extension of the traditional finite element analysis (FEA). In this method, the Non-Uniform Rational B-Splines (NURBS) are employed for the description of geometry as well as unknown field variables. As a result, in this idea, geometric design and computational analysis are linked. The IGA possesses several advantages compared to the traditional FEA due to the exclusive characteristics of NURBS, including smoothness, high-order continuity, and reduction of total degree-of-freedom [40-43].

Analytical methods provide solutions with high accuracy; however, their applications are restricted to certain types of plate problems. Abdollahzadeh Shahrbabaki and Alibeigloo [44] performed a 3D free vibration analysis of FG-CNTRC rectangular plates using the Ritz method. They reported the computed results for several combinations of boundary conditions and different geometrical and material parameters. Zhang et al. [45] employed the state-space Levy method to determine the free vibration response of FG-CNTRC plates. In their work, it is assumed that the plates are subjected to in-plane loads. They computed the plates' natural frequencies and mode shapes based on the proposed approach. By using Navier's method and in the context of the FSDT, Duc et al. [46] analyzed the static and free vibration behaviors of FG-CNTRC plates resting on elastic foundations. They presented several numerical examples to verify the accuracy of the results compared to those obtained by previous approaches.

The semi-analytical methods, which are neither analytical nor can be classified as numerical solutions, are also applied to investigate the vibrational behavior of FG-CNTRC plates. Malekzadeh and Heydarpour [47] used a 3D semi-analytical approach for static and free vibration analyses of laminated plates with FG-CNTRC layers. They assumed that each layer is fabricated from a single-walled carbon nanotubes (SWCNTs) mixture and an isotropic matrix. In their investigation, the layerwise-differential quadrature method (LW-DQM) is used to describe the displacement field in the thickness direction. Alibeigloo and Emtehani [48] obtained a closed-form solution for static and free vibration responses of FG-CNTRC plates. They used Fourier series expansion and the state space technique along the in plane and thickness directions, respectively. Wang et al. [49] employed the multi-term Kantorovich-Galerkin method to investigate free vibration and buckling behaviors of FG-CNTRC plates based on the CPT. They solved the governing equations with the state-space approach.

In addition, several numerical techniques have already been employed to study the vibrational behavior of FG-CNTRC plate structures. In this respect, Zhu et al. [5] applied the finite element method (FEM) in the context of the FSDT to evaluate natural frequencies and mode shapes for various patterns of FG-CNTRC plates. Using the element-free *kp*-Ritz method in the framework of the FSDT, Lei et al. [50] investigated free vibration analysis of laminated FG-CNTRC plates in a thermal environment. They examined the influences of various parameters such as boundary condition, CNTs volume fraction, width-to-thickness ratio, aspect ratio, and temperature change. Wu and Li [51] examine the 3D free vibration analysis of FG-CNTRC rectangular plates. They developed a unified formulation of finite prism methods (FPMs) based on Reissner's mixed variational theorem for FG-CNTRC and fiber-reinforced composite (FRC) plates. They assumed two opposite edges of the plates to be simply supported and the remaining edges to be clamped, simply supported or free. In the case of FG-CNTRC plates, they verified the solution method with the FSDT based FEM and those obtained by ANSYS software. Malekzadeh and Zarei [52] performed free vibration analysis of quadrilateral laminated FG-CNTRC plates. They discretized the governing equations according to the differential quadrature method (DQM). They investigated the effects of different related parameters. Zhang et al. applied the element-free IMLS-Ritz method to study free vibration of various FG-CNTRC plate structures with different configurations [53-55]. Using the HSDT kinematic model and FEM, Mehar et al. [56] investigated the free vibration response of FG-CNTRC plates subjected to elevated temperature. Phung-Van et al. [57] applied the isogeometric method based on the third-order shear deformation theory (TSDT) of Reddy to study the static and dynamic behaviors of FG-CNTRC plates. They compared the presented numerical values with those obtained

by other numerical approaches. Based on the FSDT, Garcia-Macias et al. [58] utilized a shell element formulated in the oblique coordinates to study the static and free vibration behaviors of FG-CNTRC skew plates. They compared the computed numerical data with those obtained by ANSYS software. The Ritz method is used by Kiani [59] in order to evaluate natural frequencies of FG-CNTRC moderately thick skew plates subjected to different boundary conditions. Ansari et al. [60] presented the generalized differential quadrature method (GDQM) based on the TSDT to analyze free vibration of FG-CNTRC thick plates with arbitrary shapes. They showed the accuracy of the proposed model through a wide range of comparison studies. Using GDQM based on FSDT, Majidi et al. [61] performed vibration analysis of cantilever FG-CNTRC trapezoidal plates. They presented the numerical results for a variety of included geometrical parameters. Mohammadi and Setoodeh [62] executed the free vibration behavior of FG-CNTRC skew folded plates. They showed that the fundamental frequency ratio increases very considerably at too high skew angles.

Heretofore, numerous HSDTs have been proposed in the literature. To the best of the authors' knowledge, the new LHSDT has not been employed to deal with different mechanical behaviors of FG-CNTRC plates. Thus, this paper aims to investigate the accuracy and reliability of the proposed LHSDT when combined with the IGA in studying vibrational behaviors of FG-CNTRC plates. The remainder of the paper is structured as follows. Section 2 provides the geometry and material description of FG-CNTRC plates. Section 3 contains the kinematic and constitutive equations of the plate. In the following, the energy formulation of the plate is provided. Section 4 represents a brief review of the basic concepts of IGA. The isogeometric model of the FG-CNTRC plate in free and forced vibration analyses is also addressed in this section. Then a comprehensive set of results is demonstrated in section 5 to show the capability and efficiency of the proposed formulation. Finally, some concluding remarks are drawn in section 6.

2. Geometry and Material Properties of the FG-CNTRC Plate

Figure 1(a) shows the geometry of an FG-CNTRC plate with length *a*, width *b*, and thickness *h*. The in-plane coordinates (*x*,*y*) are also displayed in this figure. As depicted in Fig. 1(b), it is assumed that the plate is fabricated from a polymetric matrix reinforced by SWCNTs with uniform distribution (UD) and three linear FG patterns. These patterns are denoted by FG-X, FG-O, and FG-V. The volume fraction of CNTs in the cases above are specified by [5,53,54,57,59,62]

$$\text{UD:} \quad V_{CNT}(z) = V_{CNT}^{*} \tag{1a}$$

$$\text{FG-X:} \quad V_{CNT}(z) = 4V_{CNT}^{*}\frac{|z|}{h} \tag{1b}$$

$$\text{FG-O:} \quad V_{CNT}(z) = 2V_{CNT}^{*}\left(1-\frac{2|z|}{h}\right) \tag{1c}$$

$$\text{FG-V:} \quad V_{CNT}(z) = V_{CNT}^{*}\left(1+\frac{2z}{h}\right) \tag{1d}$$

In which *z* is the thickness coordinate variable. It is also notable that all considered patterns have the same total volume fraction of CNTs, namely, V_{CNT}^{*}, which is given by [5,10,57,59,62]

$$V_{CNT}^{*} = \frac{w^{CNT}}{w^{CNT} + \dfrac{\rho^{CNT}}{\rho^{m}} - w^{CNT}\dfrac{\rho^{CNT}}{\rho^{m}}} \tag{2}$$

In Eq. (2), w^{CNT} is the mass fraction of CNTs. Moreover, ρ^{CNT} and ρ^{m} denote mass densities of CNTs and matrix, respectively.

The modified rule of mixture is adopted in order to evaluate the apparent mechanical properties of the resulting nanocomposites as [5,10,57,59,62,63]

$$\begin{aligned} E_{11} &= \eta_1 V_{CNT} E_{11}^{CNT} + V_m E^m \\ \frac{\eta_2}{E_{22}} &= \frac{V_{CNT}}{E_{22}^{CNT}} + \frac{V_m}{E^m} \\ \frac{\eta_3}{G_{12}} &= \frac{V_{CNT}}{G_{12}^{CNT}} + \frac{V_m}{G^m} \end{aligned} \tag{3}$$

where η_j, $j=1,2,3$ represent three efficiency parameters which are used to consider the size-dependent effects of CNTRC plates. These parameters for three different volume fractions of CNTs are given in Table 1 [5,10,57,62].

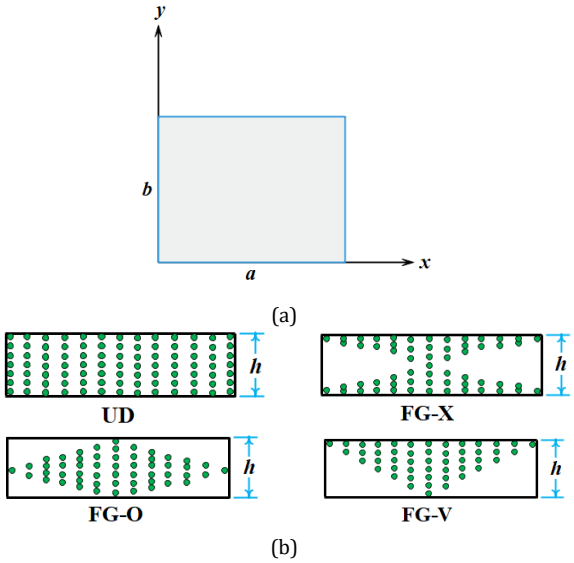

Fig. 1. (a) Geometrical model for an FG-CNTRC plate; (b) Typical distribution patterns for CNTs along with the plate thickness.

Table 1. Efficiency parameters for three different values of CNTs volume fractions [5,10,57,62].

V_{CNT}^{*}	η_1	η_2	η_3
0.11	0.149	0.934	0.939
0.14	0.150	0.941	0.941
0.17	0.149	1.381	1.381

Furthermore, $\left\{E_{11}^{CNT}, E_{22}^{CNT}, G_{12}^{CNT}\right\}$ and E^m indicate elastic moduli of the CNTs and Young modulus of the matrix, respectively. Finally, the volume fraction of CNTs and matrix, which are denoted respectively by V_{CNT} and V_m, satisfy the following condition in analogy to the relation between volume fractions of matrix and reinforcing phase in FRCs

$$V_{CNT} + V_m = 1 \tag{4}$$

The equivalent Poisson's ratio ν_{12} and the mass density ρ of the FG-CNTRC plates through the thickness are obtained using the conventional rule of mixture [5,57,59,62]

$$\nu_{12} = V_{CNT}^{*}\nu_{12}^{CNT} + V_m\nu^m \tag{5}$$

$$\rho = V_{CNT}\rho^{CNT} + V_m\rho^m \tag{6}$$

where ν_{12}^{CNT} and ν^m represent Poisson's ratio of CNT and matrix, respectively. As reported in [59], the equivalent Poisson's ratio ν_{12} is weakly dependent on the thickness coordinate z and, consequently, the distribution of CNTs.

3. The Logarithmic Higher Order Shear Deformation Theory

3.1. Kinematic and Constitutive Equations

In a general five parameters HSDT, the displacement field (u, v, w) of an arbitrary material point can be written as [64]

$$\begin{aligned} u(x,y,z,t) &= u_0(x,y,t) - z\frac{\partial w_0(x,y,t)}{\partial x} \\ &\quad + f(z)\theta_x(x,y,t) \\ v(x,y,z,t) &= v_0(x,y,t) - z\frac{\partial w_0(x,y,t)}{\partial y} \\ &\quad + f(z)\theta_y(x,y,t) \\ w(x,y,z,t) &= w_0(x,y,t) \end{aligned} \tag{7}$$

in which (u_0, v_0, w_0) and (θ_x, θ_y) express displacement components and normal rotations of a material point in the mid-plane of the plate. Besides, $f(z)$ is a kinematic function defines the distribution of transverse shear strains along the thickness of the plate. The function $f(z)$ must satisfy the tangential stress-free boundary conditions at the top and bottom surfaces of the plate. According to this condition, various forms of transverse shear functions have been proposed by many researchers during past decades. These functions include polynomial functions [27-30], trigonometric functions and their inverse [31,32], exponential function [33,34], hyperbolic functions [35,36] and combination functions [37]. Recently Zhu et al. [38] proposed a logarithmic type of function, which is used in this study

$$f(z) = \frac{1}{2}\ln\left(\frac{h-z}{h+z}\right) + \frac{4z}{3h} \tag{8}$$

For the considered distribution, one can easily check that

$$g(z) = df(z)/dz\big|_{z=\pm h/2} = 0 \tag{9}$$

Some proposed transverse shear functions are listed in Table 2 and are plotted in Fig. 2(a). Moreover, the derivative of these functions is displayed in Fig. 2(b), which confirms the condition of zero shear stress at the upper and lower surfaces of the plate.

Table 2. Some proposed transverse shear functions in the literature.

Model	Transverse shear function
Reddy [27]	$f(z) = z\left(1 - \frac{4z^2}{3h^2}\right)$
Touratier [31]	$f(z) = \frac{h}{\pi}\sin\left(\frac{\pi z}{h}\right)$
Soldatos [33]	$f(z) = h\sinh\left(\frac{z}{h}\right) - z\cosh(\frac{1}{2})$
Karama et al. [35]	$f(z) = z \times \mathrm{e}^{-2\left(\frac{z}{h}\right)^2}$
Mantari et al. [37]	$f(z) = \sin\left(\frac{\pi z}{h}\right) \times e^{\frac{1}{2}\cos\left(\pi\frac{z}{h}\right)} + \frac{\pi z}{2h}$
Zhu et al. [38]	$f(z) = \frac{1}{2}\ln\left(\frac{h-z}{h+z}\right) + \frac{4z}{3h}$

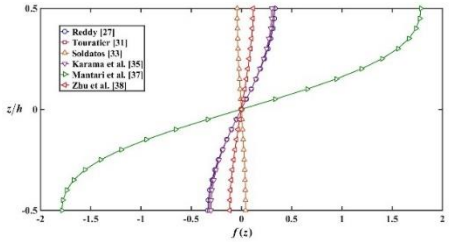

(a) Shear shape functions

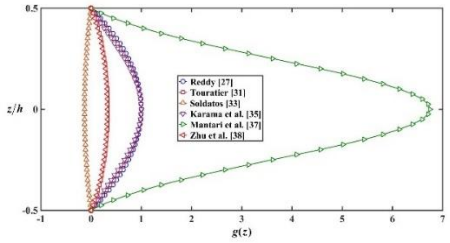

(b) Derivatives of shear shape functions

Fig. 2. (a) Some proposed shear shape functions; (b) Derivatives of the proposed shear shape functions.

The strain tensor components generated by the above displacement field are given by [65]

$$\varepsilon_p = \begin{bmatrix}\varepsilon_{xx}\\ \varepsilon_{yy}\\ \gamma_{xy}\end{bmatrix} = \begin{bmatrix}\frac{\partial u_0}{\partial x}\\ \frac{\partial v_0}{\partial y}\\ \frac{\partial u_0}{\partial y}+\frac{\partial v_0}{\partial x}\end{bmatrix} + z\begin{bmatrix}-\frac{\partial^2 w_0}{\partial x^2}\\ -\frac{\partial^2 w_0}{\partial y^2}\\ -2\frac{\partial^2 w_0}{\partial x \partial y}\end{bmatrix} + f(z)\begin{bmatrix}\frac{\partial \theta_x}{\partial x}\\ \frac{\partial \theta_y}{\partial y}\\ \frac{\partial \theta_x}{\partial y}+\frac{\partial \theta_y}{\partial x}\end{bmatrix} \quad (10)$$

$$\gamma = \begin{bmatrix}\gamma_{yz}\\ \gamma_{xz}\end{bmatrix} = g(z)\begin{bmatrix}\theta_y\\ \theta_x\end{bmatrix}$$

The non-zero strain components are usually gathered into a single vector and can be rewritten as [38,66,67]

$$\varepsilon = [\varepsilon_p \quad \gamma]^T = [\varepsilon_{xx} \quad \varepsilon_{yy} \quad \gamma_{xy} \quad \gamma_{yz} \quad \gamma_{xz}]^T = Z\hat{\varepsilon} \quad (11)$$

where

$$Z = \begin{bmatrix}1 & 0 & 0 & 0 & 0\\ 0 & 1 & 0 & 0 & 0\\ 0 & 0 & 1 & 0 & 0\\ z & 0 & 0 & 0 & 0\\ 0 & z & 0 & 0 & 0\\ 0 & 0 & z & 0 & 0\\ f(z) & 0 & 0 & 0 & 0\\ 0 & f(z) & 0 & 0 & 0\\ 0 & 0 & f(z) & 0 & 0\\ 0 & 0 & 0 & g(z) & 0\\ 0 & 0 & 0 & 0 & g(z)\end{bmatrix}^T \quad (12)$$

and

$$\hat{\varepsilon} = \begin{bmatrix}\frac{\partial u_0}{\partial x}\\ \frac{\partial v_0}{\partial y}\\ \frac{\partial u_0}{\partial y}+\frac{\partial v_0}{\partial x}\\ -\frac{\partial^2 w_0}{\partial x^2}\\ -\frac{\partial^2 w_0}{\partial y^2}\\ -2\frac{\partial^2 w_0}{\partial x \partial y}\\ \frac{\partial \theta_x}{\partial x}\\ \frac{\partial \theta_y}{\partial y}\\ \frac{\partial \theta_x}{\partial y}+\frac{\partial \theta_y}{\partial x}\\ \theta_y\\ \theta_x\end{bmatrix} \quad (13)$$

The generalized Hook's law can be expressed as [57,68-71]

$$\boldsymbol{\sigma} = \mathbf{Q}\boldsymbol{\varepsilon} \quad (14)$$

in which

$$\boldsymbol{\sigma} = \begin{bmatrix}\sigma_x\\ \sigma_y\\ \tau_{xy}\\ \tau_{yz}\\ \tau_{xz}\end{bmatrix}, \mathbf{Q} = \begin{bmatrix}Q_{11} & Q_{12} & 0 & 0 & 0\\ Q_{12} & Q_{22} & 0 & 0 & 0\\ 0 & 0 & Q_{66} & 0 & 0\\ 0 & 0 & 0 & Q_{44} & 0\\ 0 & 0 & 0 & 0 & Q_{55}\end{bmatrix} \quad (15)$$

with

$$\begin{aligned} Q_{11}(z) &= \frac{E_{11}(z)}{1-\nu_{12}(z)\nu_{21}(z)}\\ Q_{12}(z) &= \frac{\nu_{12}(z)E_{22}(z)}{1-\nu_{12}(z)\nu_{21}(z)}\\ Q_{22}(z) &= \frac{E_{22}(z)}{1-\nu_{12}(z)\nu_{21}(z)}\\ Q_{66}(z) &= G_{12}(z)\\ Q_{44}(z) &= G_{23}(z)\\ Q_{55}(z) &= G_{13}(z) \end{aligned} \quad (16)$$

3.2. Energy Formulation of the FG-CNTRC Plate

The total potential energy (Π) of the plate can be expressed as [38]

$$\Pi = U_p - T_p - U_F \quad (17)$$

The strain energy U_p of the plate can be written as

$$U_p = \frac{1}{2}\int_V \boldsymbol{\sigma}^T \boldsymbol{\varepsilon} dV = \frac{1}{2}\int_{\Omega_0}\int_{-h/2}^{h/2} \boldsymbol{\sigma}^T \boldsymbol{\varepsilon} dz d\Omega_0 \quad (18)$$

where V and Ω_0 denote the volume and mid-surface area of the plate, respectively. With the aid of Eqs. (11) and (14), Eq. (18) can be rewritten as

$$\begin{aligned} U_p &= \frac{1}{2}\int_{\Omega_0}\int_{-\frac{h}{2}}^{\frac{h}{2}} (Q\varepsilon)^T \varepsilon dz d\Omega_0\\ &= \frac{1}{2}\int_{\Omega_0}\int_{-\frac{h}{2}}^{\frac{h}{2}} \varepsilon^T Q^T \varepsilon dz d\Omega_0\\ &= \frac{1}{2}\int_{\Omega_0}\int_{-\frac{h}{2}}^{\frac{h}{2}} (Z\hat{\varepsilon})^T Q Z\hat{\varepsilon} dz d\Omega_0\\ &= \frac{1}{2}\int_{\Omega_0}\int_{-\frac{h}{2}}^{\frac{h}{2}} \hat{\varepsilon}^T Z^T Q Z\hat{\varepsilon} dz d\Omega_0\\ &= \frac{1}{2}\int_{\Omega_0} \hat{\varepsilon}^T C\, \hat{\varepsilon} d\Omega_0 \end{aligned} \quad (19)$$

where **C** is the matrix of elastic constants, which is defined by

$$C = \int_{-\frac{h}{2}}^{\frac{h}{2}} Z^T Q Z dz \tag{20}$$

By substituting of Eqs. (12) and (15), one can obtain

$$C = \begin{bmatrix} A & B & E & 0 \\ B & D & F & 0 \\ E & F & H & 0 \\ 0 & 0 & 0 & A^s \end{bmatrix} \tag{21}$$

with

$$\begin{aligned} &\left(A_{ij}, B_{ij}, D_{ij}, E_{ij}, F_{ij}, H_{ij}\right) \\ &= \int_{-h/2}^{h/2} \left(1, z, z^2, f(z), zf(z), f^2(z)\right) Q_{ij}(z) dz, \\ &i, j = 1, 2, 6 \\ &A_{ij}^s = \int_{-h/2}^{h/2} g^2(z) Q_{ij}(z) dz, \\ &i, j = 4, 5 \end{aligned} \tag{22}$$

The kinetic energy T_p is given by [38]

$$T_p = \frac{1}{2}\int_V \dot{\mathbf{U}}^T \rho \dot{\mathbf{U}} dV = \frac{1}{2}\int_{\Omega_0}\int_{-h/2}^{h/2} \dot{\mathbf{U}}^T \rho \dot{\mathbf{U}} dz d\Omega_0 \tag{23}$$

In which **U** is the global displacement vector defined by

$$U = \Theta \bar{u} \tag{24}$$

with

$$\mathbf{\Theta} = \begin{bmatrix} 1 & 0 & 0 & z & 0 & 0 & f(z) & 0 & 0 \\ 0 & 1 & 0 & 0 & z & 0 & 0 & f(z) & 0 \\ 0 & 0 & 1 & 0 & 0 & 0 & 0 & 0 & 0 \end{bmatrix}$$

$$\bar{\mathbf{u}} = \begin{bmatrix} u \\ v \\ w \\ -\partial w_0/\partial x \\ -\partial w_0/\partial y \\ 0 \\ \theta_x \\ \theta_y \\ 0 \end{bmatrix} \tag{25}$$

By substituting Eq. (24) into Eq. (23), one can write

$$\begin{aligned} T_p &= \frac{1}{2}\int_{\Omega_0}\int_{-\frac{h}{2}}^{\frac{h}{2}} (\Theta\dot{u})^T \rho (\Theta\dot{u}) dz d\Omega_0 \\ &= \tfrac{1}{2}\int_{\Omega_0}\int_{-\frac{h}{2}}^{\frac{h}{2}} \dot{u}^T \Theta^T \rho \Theta \dot{u} dz d\Omega_0 \end{aligned} \tag{26}$$

Therefore, the kinetic energy of the plate can be expressed by

$$T_p = \tfrac{1}{2}\int_{\Omega_0} \dot{u}^T m \dot{u} dz d\Omega_0 \tag{27}$$

where

$$m = \begin{bmatrix} m_1 & m_2 & m_4 \\ m_2 & m_3 & m_5 \\ m_4 & m_5 & m_6 \end{bmatrix} \tag{28}$$

with

$$\begin{aligned} &(m_1, m_2, m_3, m_4, m_5, m_6) = \\ &I\int_{-\frac{h}{2}}^{\frac{h}{2}} (1, z, z^2, f(z), zf(z), f^2(z))\, \rho(z) dz \end{aligned} \tag{29}$$

in which **I** is the identity matrix of order 3×3.

Finally, the work generated by the external transverse load $\hat{p}$ is calculated by

$$U_F = \frac{1}{2}\int_{\Omega_0} w_0 \hat{p} d\Omega_0 \tag{30}$$

4. Isogeometric Model of FG-CNTRC Plates

In this section, the isogeometric model for studying the vibrational behavior of FG-CNTRC plates is demonstrated.

4.1. Basic Definitions

In this sub-section, some fundamental concepts of the IGA are reviewed. To have a detailed study, one can refer to [39,72]. In order to generate B-splines and NURBS basis functions, a knot vector must be defined, which is a non-decreasing set of numbers, represented as $\mathbf{\Xi} = \{\xi_1, \xi_2, ..., \xi_{n+p+1}\}$. In this definition, ξ_i is the *i-th* knot, *n* denotes the number of basis functions, and *p* stands for the polynomial order. This study uses open and uniform knot vectors, which means that the knots are equally spaced. Moreover, the first and last knots are repeated *p*+1 times. The univariate B-spline basis functions $N_{i,p}$ are produced by inserting knot values into the well-known Cox-de Boor recursion formula, starting with the zeroth-order (*p*=0) basis function as [73,74]

$$N_{i,0}(\xi) = \begin{cases} 1 & \text{if } \xi_i \le \xi \le \xi_{i+1} \\ 0 & \text{otherwise} \end{cases} \tag{31a}$$

and for $p \ge 1$

$$\begin{aligned} N_{i,p}(\xi) &= \frac{\xi - \xi_i}{\xi_{i+p} - \xi_i} N_{i,p-1}(\xi) \\ &+ \frac{\xi_{i+p+1} - \xi}{\xi_{i+p+1} - \xi_{i+1}} N_{i+1,p-1}(\xi) \end{aligned} \tag{31b}$$

It should be indicated that for p=0, 1, the generated polynomials are identical to those considered in the standard FEM. However, they are different for higher-order basis functions.

A B-Spline curve of degree p is defined as follows

$$C(\xi) = \sum_{i=1}^{n} N_{i,p}(\xi) P_i \tag{32}$$

where $\mathbf{P_i} = \left\{P_{ix}, P_{iy}\right\}^T$ are coordinate positions of the i-th control point.

A B-spline surface is easily obtained by the tensor product of two univariate basis functions of order p and q, respectively constructed on two-knot vectors of $\boldsymbol{\Xi} = \left\{\xi_1, \xi_2, ..., \xi_{n+p+1}\right\}$ and $\mathbf{H} = \left\{\eta_1, \eta_2, ..., \eta_{m+q+1}\right\}$. This definition is mathematically expressed by

$$\mathbf{S}(\xi,\eta) = \sum_{i=1}^{n}\sum_{j=1}^{m} N_{i,p}(\xi) M_{j,q}(\eta) \mathbf{P}_{i,j} \tag{33}$$

where $N_{i,p}(\xi)$ and $M_{j,q}(\eta)$ are two univariate B-spline basis functions in ξ and η directions, respectively. Also, $\mathbf{P}_{i,j}$ is a $n \times m$ net of control points.

Equation (33) is typically rewritten in the familiar notation which is used in finite element

$$\mathbf{S}(\xi,\eta) = \sum_{I=1}^{n\times m} N_I(\xi,\eta) \mathbf{P}_I \tag{34}$$

where $N_I(\xi,\eta) = N_{i,p}(\xi) M_{j,q}(\eta)$ is the basis function corresponding to the control point I.

To exactly describe the geometric model of various objects such as conic sections, NURBS are defined. In two-dimensional space, a NURBS surface is defined as

$$\mathbf{S}(\xi,\eta) = \sum_{I=1}^{n\times m} R_I(\xi,\eta)\mathbf{P}_I \text{ with}$$
$$R_I(\xi,\eta) = \frac{N_I(\xi,\eta) w_I}{\sum_{I=1}^{n\times m} N_I(\xi,\eta) w_I} \tag{35}$$

in which w_I is the weighting coefficient associated with the I-th control point. These numerical values control the flexibility of the surface at the control point location.

4.2. Discretization of Field Equations

The field equations are discretized using NURBS basis functions as follows

$$u(\xi,\eta) = \sum_{I=1}^{n_{CP}} R_I(\xi,\eta)\, q_I \tag{36}$$

where n_{CP} is the number of control points for the whole plate and $\mathbf{q}_I = [u_I \quad v_I \quad w_I \quad \theta_{xI} \quad \theta_{yI}]^T$ is the vector of nodal displacements associated with the control point I.

Substitution of Eq. (36) respectively into Eqs. (18), (23) and (30), then the resulting expressions into Eq. (17), and finally using Hamilton's principle, the vibrational behavior is described by the following matrix form

$$M\ddot{q} + Kq = F \tag{37}$$

where $\mathbf{K}$ is the stiffness matrix, $\mathbf{M}$ is the mass matrix, and $\mathbf{F}$ is the load vector. They are respectively expressed by

$$\begin{aligned} K &= \int_{\Omega_0} B_k^T C B_k d\Omega_0 \\ M &= \int_{\Omega_0} B_m^T m B_m d\Omega_0 \\ F &= \int_{\Omega_0} \hat{p} N d\Omega_0 \end{aligned} \tag{38}$$

with

$$\mathbf{B}_k^I = \begin{bmatrix} R_{I,x} & 0 & 0 & 0 & 0 \\ 0 & R_{I,y} & 0 & 0 & 0 \\ R_{I,y} & R_{I,x} & 0 & 0 & 0 \\ 0 & 0 & -R_{I,xx} & 0 & 0 \\ 0 & 0 & -R_{I,yy} & 0 & 0 \\ 0 & 0 & -2R_{I,xy} & 0 & 0 \\ 0 & 0 & 0 & R_{I,x} & 0 \\ 0 & 0 & 0 & 0 & R_{I,y} \\ 0 & 0 & 0 & R_{I,y} & R_{I,x} \\ 0 & 0 & 0 & 0 & R_I \\ 0 & 0 & 0 & R_I & 0 \end{bmatrix}$$

$$\mathbf{B}_m^I = \begin{bmatrix} R_I & 0 & 0 & 0 & 0 \\ 0 & R_I & 0 & 0 & 0 \\ 0 & 0 & R_I & 0 & 0 \\ 0 & 0 & -R_{I,x} & 0 & 0 \\ 0 & 0 & -R_{I,y} & 0 & 0 \\ 0 & 0 & 0 & 0 & 0 \\ 0 & 0 & 0 & R_I & 0 \\ 0 & 0 & 0 & 0 & R_I \\ 0 & 0 & 0 & 0 & 0 \end{bmatrix} \tag{39}$$

$$\mathbf{N}^I = \begin{bmatrix} 0 & 0 & R_I & 0 & 0 \end{bmatrix}^T$$

4.3. Time Marching

The time-dependent part of the problem is solved using the Newmark scheme. In this approach, it is assumed that the initial state $t = t_0$ is known as $(\mathbf{q}_0, \dot{\mathbf{q}}_0, \ddot{\mathbf{q}}_0)$. Knowing the predetermined initial state, the dynamic responses at the time $t_1 = t_0 + \Delta t$, i.e., $(\mathbf{q}_1, \dot{\mathbf{q}}_1, \ddot{\mathbf{q}}_1)$ are obtained as [75]

$$\begin{aligned} &\hat{K} q_1 = \hat{F} \\ &\ddot{q}_1 = a_0(q_1 - q_0) - a_1\dot{q}_0 - a_2\ddot{q}_0 \\ &\dot{q}_1 = \dot{q}_0 + a_3\ddot{q}_0 + a_4\ddot{q}_1 \end{aligned} \tag{40}$$

where

$$\hat{K} = a_0 M + K \tag{41}$$

and

$$\hat{F} = F_1 + M(a_0 q_0 + a_1 \dot{q}_0 + a_2 \ddot{q}_0) \tag{42}$$

with

$$a_0 = \frac{1}{\beta \Delta t^2}; \quad a_1 = a_0 \Delta t; \quad a_2 = \frac{1}{2\beta} - 1; \quad a_3 = (1-\delta)\Delta t; \quad a_4 = \delta \Delta t \tag{43}$$

The existing coefficients in Eq. (43) are assumed to be $\beta = 0.25$ and $\delta = 0.5$.

5. Numerical Results

In this section, the current numerical approach is verified. For this purpose, several numerical examples are presented to investigate the vibrational behavior of FG-CNTRC plates. The results are separately presented in two sub-sections, respectively, for the free and forced vibration analyses. In all the examples, quartic order ($p = q = 4$) NURBS basis functions are used for the geometric description of the plate. Several combinations of simply supported (S), clamped (C), and free (F) boundaries are considered for the FG-CNTRC plate. For simply supported and clamped edges, we have [38]

Simply supported boundaries:

$$v = w_0 = \theta_y = 0, \quad \text{at } x=0,\ a$$
$$u = w_0 = \theta_x = 0, \quad \text{at } y=0,\ b \tag{44}$$

Clamped boundaries:

$$u = v = w_0 = \theta_x = \theta_y = \partial w_0 / \partial n = 0,$$
at $x=0,\ a$ and $y=0,\ b$

It should be noted that the condition $\partial w_0 / \partial n = 0$ is implied by fixing the adjacent control points of the corresponding boundary.

In this study, the poly{(m-phenylenevinylene) - co - [(2,5-dioctoxy-p-phenylene) vinylene]} referred to PmPV is considered as the matrix and the (10,10) SWCNTs are chosen as the reinforcement of FG-CNTRC plates. The material properties of these constituents at room temperature (T=300K) are listed in Table 3 [5,10,57,62]. Moreover, it is assumed that $G_{13} = G_{23} = G_{12}$ [5,57,62]. In addition, the non-dimensional frequency parameter and central deflections are defined as

$$\lambda = \omega (b^2/h)\sqrt{\rho^m / E^m}$$
$$\bar{w}_c = 10^3 w_c E h^3 / \hat{p}_0 b^4$$
$$\tilde{w}_c = 10^2 w_c E_2 h^3 / \hat{p}_0 b^4 \tag{45}$$
$$\hat{w}_c = 10^3 w_c E^m h^3 / \hat{p}_0 b^4$$

where $\hat{p}_0$ is the intensity of the applied transverse loading.

5.1. Free Vibration Analysis

Firstly, it is necessary to investigate the convergence and stability of the proposed formulation by performing the convergence study and comparing the results with those available in the open literature. The fundamental frequency parameter for various types of supported FG-CNTRC plates with CNT volume fraction $V_{CNT}^* = 0.11$ are listed in Table 4. It can be observed that the convergence behavior is very excellent, and the converged values are obtained by considering only five elements in each direction of the parametric coordinate. Besides, the computed results for different with-to-thickness ratios are simultaneously compared with those extracted by other solution methods; analytical methods [46], semi-analytical methods [48], and numerical techniques [5,50,51,57,62]. The present solution is very close to the semi-analytical method conducted by Alibeigloo and Emtehani [48] and the 3D-based FPM reported by Wu and Li [51].

Moreover, the computed results are in good agreement with those obtained by other approaches based on different plate models [5,46,50,57,62]. In another comparison study, Table 5 provides natural frequencies corresponding to the first three modes of vibration for UD, FG-X, and FG-O CNTRC plates having different types of boundary conditions. The parameters of the plates are taken to be $a/b = 1$ $b/h = 100$, $V_{CNT}^* = 0.11$. The computed data are compared with the results obtained by Wang et al. [49] via the Kantorovich-Galerkin method in the context of the CPT. Again, the accuracy and effectiveness of the method are evident by considering the fact that the present solution generates the lower bounds in all the considered modes.

Table 3. Material properties of (10,10) SWCNTs and PmPV matrix at the room temperature (300 K) [5,10,57,62].

(10, 10) SWCNTs	(PmPV) matrix
$E_{11}^{CNT} = 5.6466$ TPa	$E^m = 2.1$ GPa
$E_{22}^{CNT} = 7.0800$ TPa	$\nu^m = 0.34$
$G_{12}^{CNT} = 1.9445$ TPa	$\rho^m = 1150$ kg/m^3
$\rho^{CNT} = 1400$ kg/m^3	
$\nu_{12}^{CNT} = 0.175$	

Table 4. Convergence and comparison study of fundamental frequency parameter $\left(\lambda = \omega(b^2/h)\sqrt{\rho^m/E^m}\right)$ for various types of simply supported FG-CNTRC plates with different CNT volume fractions $\left(a/b = 1,\ V^*_{CNT} = 0.11\right)$.

b/h	Method	$N_\xi = N_\eta$	Distribution pattern			
			UD	FG-X	FG-O	FG-V
10	Present	1	13.5505	14.6702	11.3785	12.4563
		3	13.5487	14.6687	11.3766	12.4544
		5	13.5486	14.6685	11.3765	12.4542
		7	13.5486	14.6685	11.3765	12.4542
		9	13.5486	14.6685	11.3765	12.4542
	Analytical [46]		---	14.064	10.779	11.732
	Semi-analytical [48]		13.555	14.668	11.332	12.263
	FEM (FSDT) [5]		13.532	14.616	11.550	12.452
	Element-free *kp*-Ritz method (FSDT) [50]		13.495	14.578	11.514	12.416
	IGA (TSDT) [57]		14.024	15.254	11.773	12.755
20		1	17.3158	19.9069	13.4256	15.0749
		3	17.3122	19.9031	13.4226	15.0717
		5	17.3120	19.9029	13.4224	15.0714
		7	17.3120	19.9029	13.4224	15.0714
		9	17.3120	19.9029	13.4224	15.0714
	Analytical [46]		---	18.571	12.316	13.855
	FEM (FSDT) [5]		17.355	19.939	13.523	15.110
	IGA (TSDT) [57]		17.503	20.241	13.500	15.127
50	Present	1	19.1597	22.9026	14.2548	16.2047
		3	19.1548	22.8968	14.2512	16.2007
		5	19.1545	22.8964	14.2510	16.2003
		7	19.1545	22.8964	14.2510	16.2003
		9	19.1545	22.8964	14.2510	16.2003
	Analytical [46]		---	20.959	12.895	14.716
	Semi-analytical [48]		19.168	22.898	14.280	16.208
	IGA (CPT) [62]		19.5813	23.6446	14.2484	16.4471
	FEM (FSDT) [5]		19.223	22.984	14.302	16.252
	IGA (TSDT) [57]		19.093	22.880	14.153	16.093
	FPM (3D solution) [51]		19.1547	22.9020	14.2370	16.1758

Table 5. Comparison study of first three frequency parameters $\left(\lambda = \omega(b^2/h)\sqrt{\rho^m/E^m}\right)$ for UD, FG-X, and FG-O CNTRC plates with different boundary conditions $\left(a/b=1\ \ b/h=100,\ \ V^*_{CNT}=0.11\right)$.

Boundary condition	Method	Mode	Distribution pattern		
			UD	FG-X	FG-O
FSFS	Present	1	2.8839	2.9813	2.8123
		2	4.8353	4.9974	4.7056
		3	11.5308	11.9190	11.2471
	Wang et al. [49]	1	2.885	2.982	2.812
		2	4.840	5.003	4.709
		3	11.537	11.926	11.248
SSFS	Present	1	3.4781	3.5946	3.3897
		2	12.1730	12.5797	11.8758
		3	26.5833	27.4691	22.1269
	Wang et al. [49]	1	3.480	3.597	3.390
		2	12.181	12.589	11.877
		3	26.616	27.507	22.203
CSFS	Present	1	7.6637	9.0278	6.0065
		2	14.1117	15.2166	13.0183
		3	27.6422	28.8974	26.5876
	Wang et al. [49]	1	7.684	9.061	6.015
		2	14.135	15.251	13.029
		3	27.688	28.955	26.613
FCFC	Present	1	6.5380	6.7567	6.3803
		2	7.8299	8.0913	7.6327
		3	18.0045	18.6062	17.5700
	Wang et al. [49]	1	6.543	6.762	6.382
		2	7.840	8.103	7.639
		3	18.031	18.636	17.585
CCCC	Present	1	42.5275	50.9762	31.2851
		2	46.4807	54.5031	36.2900
		3	56.4779	63.7455	47.9855
	Wang et al. [49]	1	43.656	52.969	31.738
		2	47.576	56.451	36.716
		3	57.497	65.564	48.383
CCSC	Present	1	30.2226	36.2246	22.4526
		2	35.5394	41.0252	28.9664
		3	47.8413	52.6696	42.6551
	Wang et al. [49]	1	30.662	37.011	22.623
		2	35.961	41.786	29.121
		3	48.253	53.389	42.820

After successively validating the proposed formulation, the effects of various geometrical and material parameters on the non-dimensional frequency parameters of FG-CNTRC plates are studied. Table 6 investigates the influences of CNTs distribution and their volume fraction on the fundamental frequency parameter of FG-CNTRC plates. The results are prepared for square moderately thick plates $(a/b=1,\ b/h=10)$ subjected to different types of boundary conditions. It can be seen that by increasing the CNT volume fraction, the fundamental natural frequency changes significantly. This is possibly due to an increase in the stiffness of the FG-CNTRC plate when more CNTs are dispersed into the background phase.

Moreover, one can observe that, for all cases under consideration, the FG-X and FG-O distributions of CNTs give the greatest and lowest natural frequencies, respectively. Accordingly, it can be deduced that when the regions near the top and bottom surfaces of the plate are enriched with more CNTs, the flexural rigidity and, consequently, the natural frequency of the plate increases. In addition, the effect of boundary conditions is examined in this table. The presented data reveals that the CFFF and CCCC plates possess the lowest and highest vibration frequency. Thus, it can be stated that when all other geometrical and material parameters are kept constant, plates with more constrained edges have higher natural frequencies. Finally, it can be concluded that, compared with the effects of CNTs distribution, CNTs volume fraction, and boundary condition, the CNTs distribution has a lower influence on the fundamental frequency parameter of the plate.

It will be substantial to consider the effect of the width-to-thickness ratio on the frequency parameters of CNTRC plates having different FG patterns. In this study, five relative width-to-thickness ratios $(b/h=5,\ 10,\ 20,\ 50,\ 100)$ are considered. The first six frequency parameters for SSSS and CCCC plates with CNT volume fraction $V_{CNT}^{*}=0.17$ are exhibited in Table 7. It can be observed that when we move from thin $(b/h=100)$ to thick $(b/h=5)$ plates, remarkable drops occur in the frequency parameters. It can also be seen that for $b/h=5$, the frequency parameters are close to each other for all the CNTs distribution. Thus, it can be deduced that the effect of CNTs distribution is insignificant when the plate is comparably thick. These conclusions are true for two considered boundary conditions.

Table 6. The fundamental frequency parameter $\left(\lambda=\omega(b^2/h)\sqrt{\rho^m/E^m}\right)$ for various patterns of FG-CNTRC plates with different CNT volume fractions subjected to different types of boundary conditions $\left(a/b=1,\ b/h=10\right)$.

Boundary condition	V_{CNT}^{*}	Distribution pattern			
		UD	FG-X	FG-O	FG-V
SSSS	0.11	13.5486	14.6685	11.3765	12.4542
	0.14	14.3513	15.3895	12.1732	13.2774
	0.17	16.8297	18.1733	14.1343	15.4474
CCCC	0.11	18.6139	19.3399	16.7479	18.0751
	0.14	19.3053	19.9684	17.4754	18.8295
	0.17	23.2131	24.0150	21.0217	22.5522
CSCC	0.11	16.4770	17.3325	14.6043	15.7524
	0.14	17.1816	17.9815	15.3267	16.5020
	0.17	20.5269	21.5398	18.2500	19.6260
CSSS	0.11	13.9654	15.0702	11.8619	12.9187
	0.14	14.7570	15.7918	12.6352	13.7273
	0.17	17.3552	18.7014	14.7320	16.0384
CCFF	0.11	5.6700	6.3689	4.5126	5.0379
	0.14	6.1226	6.8180	4.9032	5.4645
	0.17	7.0225	7.8801	5.5778	6.2246
CFCF	0.11	6.1376	6.3092	6.0164	6.1714
	0.14	6.2466	6.4839	6.0783	6.2879
	0.17	7.6793	8.0582	7.4295	7.7550
CFFF	0.11	1.0197	1.0534	0.9952	1.0256
	0.14	1.0378	1.0843	1.0041	1.0450
	0.17	1.2758	1.3501	1.2256	1.2889

It is also worthwhile to investigate the variation of frequency parameters as the plate aspect ratio (a/b) is varied. Table 8 contains the first six frequency parameters for different configurations of simply supported and fully clamped FG-CNTRC plates with $b/h=10$ and $V_{CNT}^{*}=0.17$ having different aspect ratios $(a/b=1,\ 1.5,\ 2)$. It can be seen that for all considered patterns of CNTs and certain values of width-to-thickness ratio and volume fraction, the frequency parameters drop remarkably as the aspect ratio increases.

5.2. Forced Vibration Analysis

In this section, the transient response of FG-CNTRC plates subjected to a distributed transverse load is demonstrated.

Firstly, the comparison study is performed for two examples. In the first one, we consider a homogeneous plate which is simply supported all around and subjected to a uniformly distributed step load of intensity $\hat{p}_0$. The parameters of the plate are given by

$a=b=0.25\text{m},\ b/h=10,\ E=21\text{GPa},$

$\nu=0.25,\ \rho=800\,\text{kg}/\text{m}^3$

Figure 3 shows the variation of non-dimensional central deflection $(\bar{w}_c)$ versus time. The computed results are simultaneously compared with the FEM solution executed by Reddy [76]. An excellent agreement is revealed between both sets of results which demonstrates the capability of the proposed numerical approach to capture the temporal response of the plate.

Table 7. The first six non-dimensional frequency parameters $\left(\lambda=\omega(b^2/h)\sqrt{\rho^m/E^m}\right)$ for various patterns of simply supported and fully clamped FG-CNTRC plates have a different width-to-thickness ratio $\left(a/b=1,\ V_{CNT}^{*}=0.17\right)$.

b/h	Mode	SSSS				CCCC			
		UD	FG-X	FG-O	FG-V	UD	FG-X	FG-O	FG-V
5	1	10.9189	11.2557	10.0091	10.6149	14.2568	14.6841	13.1082	14.1829
	2	12.1538	12.2406	12.2406	12.2382	19.8667	20.3033	19.1084	19.9120
	3	12.1538	12.2406	12.2406	12.2382	23.3180	23.5147	23.5147	23.4976
	4	15.9014	16.3453	15.3050	15.8541	27.4858	28.6501	24.1766	27.3102
	5	23.2366	23.4323	21.5729	23.2719	28.6429	29.0588	28.1268	28.7991
	6	23.4920	24.0826	23.4323	23.3866	30.8184	31.6067	28.2331	30.7553
10	1	16.8297	18.1733	14.1343	15.4474	23.2131	24.0150	21.0217	22.5522
	2	22.0023	23.3221	19.9756	21.2329	29.6686	30.6881	27.8499	29.3387
	3	24.3076	24.4812	24.4812	24.4800	42.2209	43.5286	40.7311	42.2372
	4	24.3076	24.4812	24.4812	24.4800	45.7487	47.0295	41.3607	44.7372
	5	33.9269	35.4487	32.3595	33.7498	46.6360	47.1994	45.7015	47.0122
	6	41.0828	42.4255	36.9195	39.5148	49.6034	51.1210	47.0295	48.8709
20	1	21.3979	24.6024	16.5379	18.5837	35.9828	38.7426	30.1754	33.0916
	2	26.5680	29.5479	22.6224	24.6132	41.7247	44.5474	36.6482	39.5135
	3	39.6898	42.7031	36.5340	38.7809	55.1716	58.3193	50.8844	53.9061
	4	48.6152	48.9623	48.9623	48.9617	76.2045	79.9479	66.3736	71.9371
	5	48.6152	48.9623	48.9623	48.9617	76.2706	80.2275	70.3103	75.7489
	6	60.3951	63.9225	53.2979	58.7331	79.6238	83.5865	72.3239	75.7675
50	1	23.6068	28.2655	17.4918	19.9179	48.9376	57.0414	36.9501	41.8914
	2	28.8077	33.1633	23.6808	26.0667	54.0493	61.8894	43.1638	47.9762
	3	42.3600	46.6015	38.1759	40.8859	66.8718	74.4535	57.5791	62.4560
	4	64.7746	69.6027	60.7219	64.2905	88.9765	96.7396	80.8206	86.2492
	5	86.3863	101.2261	64.2266	73.1467	119.9988	128.5968	93.7105	105.4651
	6	89.0474	101.5366	67.7032	76.4772	121.0650	137.2946	97.4892	109.0781
100	1	23.9853	28.9422	17.6431	20.1351	52.4004	62.8907	38.3994	43.9303
	2	29.1946	33.8388	23.8495	26.3049	57.4093	67.5611	44.5783	49.9683
	3	42.8158	47.3199	38.4370	41.2292	70.0416	79.7311	59.0046	64.4312
	4	65.5165	70.6188	61.2604	64.9589	92.1967	101.8170	82.5360	88.5229
	5	91.6894	102.9894	66.4282	76.2611	123.8361	134.1504	101.5261	116.1646
	6	94.4276	110.5898	69.9674	79.6720	138.3135	164.4419	105.3397	119.8165

Table 8. The first six non-dimensional frequency parameters $\left(\lambda=\omega(b^2/h)\sqrt{\rho^m/E^m}\right)$ for various patterns of simply supported and fully clamped FG-CNTRC plates have a different aspect ratio $\left(b/h=10,\ V^*_{CNT}=0.17\right)$.

a/b	Mode	SSSS				CCCC			
		UD	FG-X	FG-O	FG-V	UD	FG-X	FG-O	FG-V
1.0	1	16.8297	18.1733	14.1343	15.4474	23.2131	24.0150	21.0217	22.5522
	2	22.0023	23.3221	19.9756	21.2329	29.6686	30.6881	27.8499	29.3387
	3	24.3076	24.4812	24.4812	24.4800	42.2209	43.5286	40.7311	42.2372
	4	24.3076	24.4812	24.4812	24.4800	45.7487	47.0295	41.3607	44.7372
	5	33.9269	35.4487	32.3595	33.7498	46.6360	47.1994	45.7015	47.0122
	6	41.0828	42.4255	36.9195	39.5148	49.6034	51.1210	47.0295	48.8709
1.5	1	9.5878	10.6265	7.9529	8.7255	15.2301	16.0076	13.6379	14.6173
	2	16.2051	16.3208	15.6637	16.3204	23.8975	24.8936	22.6756	23.7110
	3	16.7919	17.8521	16.3208	16.5258	28.5707	29.6788	25.6880	27.5779
	4	24.3076	24.4812	21.3922	23.1620	34.2701	35.4971	31.8794	33.6662
	5	24.7563	26.1551	24.4812	24.4800	38.3499	39.6338	37.2924	38.4841
	6	28.6662	30.0548	25.9300	27.5850	42.9736	43.3461	40.3894	43.3316
2.0	1	6.6420	7.3870	5.6556	6.1533	11.7567	12.4949	10.5690	11.2948
	2	12.1538	12.2406	12.2406	12.2404	20.6276	21.6457	18.3472	19.7098
	3	15.0954	15.9771	14.1343	15.0597	21.8099	22.7694	20.8897	21.7587
	4	16.8298	18.1734	14.3465	15.4474	27.8821	29.0346	26.1123	27.4354
	5	22.0024	23.3222	19.9756	21.2330	31.8836	33.1207	28.5903	30.6853
	6	24.3076	24.4812	24.4812	24.4800	37.0588	38.3190	34.3944	36.3522

$$\hat{p}(x,y,t)=\hat{p}_0\sin(\frac{\pi x}{a})\sin(\frac{\pi y}{b})\varphi(t) \qquad (46)$$

In the next example, a laminated plate with $a=b=0.25\text{m},\ h=0.01\text{m}$ which is subjected to suddenly applied step load is considered. It is assumed that each lamina has the following material properties

$$E_2=21\text{GPa},\ E_1=25E_2,\ G_{12}=G_{13}=0.5E_2,$$
$$G_{23}=0.2E_2,\ \nu_{12}=0.25,\ \rho=800\,\text{kg/m}^3$$

Figure 4 plots non-dimensional central deflection $(\tilde{w}_c)$ for CCFF and CFFF laminated square plates with the ply arrangement of $\left[0^\circ/90^\circ\right]$ against time. The transient solutions are compared with those obtained by Maleki et al. [77]. They employed the GDQM according to the FSDT to generate their results. Again, it can be observed that a very good agreement exists between the present solution and those reported in Ref. [77].

In the following, the dynamical load $\hat{p}$ is defined as

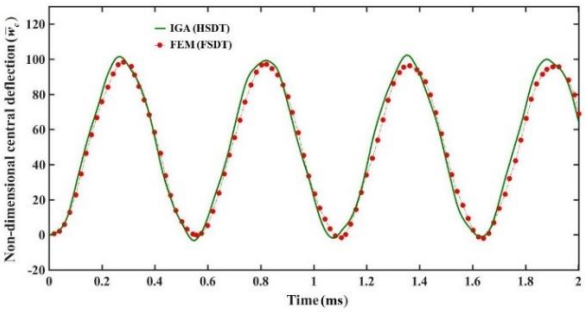

Fig. 3. Non-dimensional central deflection $(\tilde{w}_c)$ of the simply supported homogeneous plate under step uniform load $\left(a=b=0.25\text{m},\ h=0.025\text{m},\ E=21\text{GPa},\ \nu=0.25,\ \rho=800\,\text{kg/m}^3\right)$.

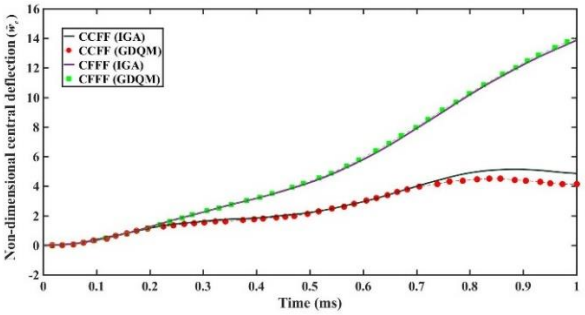

Fig. 4. Non-dimensional central deflection ($\widetilde{w}_c$) of CCFF and CFFF $\left[0^\circ/90^\circ\right]$ laminated square plates under step uniform load $\left(a=b=0.25\text{m},\ h=0.01\text{m},\ E_2=21\text{GPa},\ E_1=25E_2,\ G_{12}=G_{13}=0.5E_2,\ G_{23}=0.2E_2,\ \nu_{12}=0.25,\ \rho=800\,\text{kg/m}^3\right)$.

where $\varphi(t)$ is a function of the time variable t as

Step loading:
$$\varphi(t)=\begin{cases}1 & 0\le t\le t_1\\ 0 & t>t_1\end{cases} \tag{47a}$$

Triangular loading:
$$\varphi(t)=\begin{cases}1-t/t_1 & 0\le t\le t_1\\ 0 & t>t_1\end{cases} \tag{47b}$$

Sinusoidal loading:
$$\varphi(t)=\begin{cases}\sin\left(\pi t/t_1\right) & 0\le t\le t_1\\ 0 & t>t_1\end{cases} \tag{47c}$$

Explosive blast loading:
$$\varphi(t)=e^{-\hat{\gamma}t} \tag{47d}$$

with $t_1=0.002\text{s},\ \hat{\gamma}=330\text{s}^{-1},\ \hat{p}_0=0.1\text{MPa}$.

It is worth noting that, for the step, triangular and sinusoidal loadings, it is assumed that the plates are subjected to the aforementioned dynamical loads in the interval of 0 to t_1. After that, the load is eliminated, and the plates vibrate freely. However, in the case of explosive blast loading, it is assumed that the load is continuously applied to the plate.

Figures 5-8 investigate the influences of different FG patterns of CNTs on the non-dimensional central deflection ($\hat{w}_c$) of the plates when they are subjected to dynamical step, triangular, sinusoidal, and explosive blast loadings. The plates are characterized by $a=b=0.25\text{m},\ b/h=10$. It can be deduced that plates with FG-X and FG-O shapes have the upper and lower bounds for the central deflections and period of vibration, which is considered as a superior result in engineering design. As expected, the dynamic response of UD plates lies between the FG-X and FG-O ones. Thus, it can be concluded that the distribution of CNTs at the top and bottom surfaces of the plate is more beneficial than the dispersion of CNTs at the mid-surface.

Another study assumed that plates with the same geometrical configuration and different CNTs volume fraction are subjected to loading the above types. Moreover, the distribution pattern of FG-X is considered for the plates to account for the lower bound of deflection. Subsequently, the time histories of non-dimensional central deflection of plates ($\hat{w}_c$) are plotted in Figs. 9-12. It can be observed that for a given pattern when CNTs volume fraction increases, the amplitude of vibration decreases noticeably. As a result, it can be expressed that the appropriate selection of FG patterns for CNTs and their volume fraction can improve the passive vibrational behavior of FG-CNTRC plates.

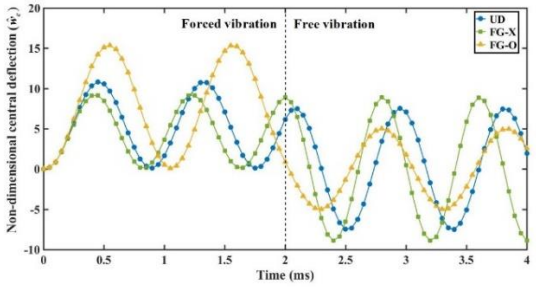

Fig. 5. Non-dimensional central deflection ($\hat{w}_c$) of the simply supported FG-CNTRC plates with various patterns subjected to the step loading $\left(a=b=0.25\text{m},\ b/h=10,\ V^*_{CNT}=0.11\right)$.

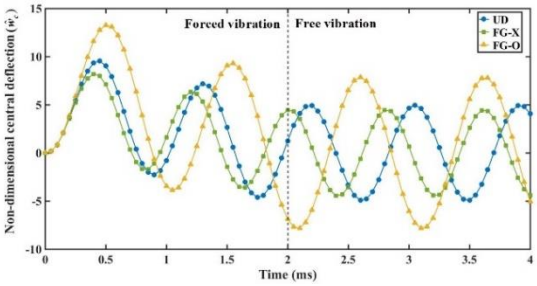

Fig. 6. Non-dimensional central deflection ($\hat{w}_c$) of the simply supported FG-CNTRC plates with various patterns subjected to the triangular loading $\left(a=b=0.25\text{m},\ b/h=10,\ V^*_{CNT}=0.11\right)$.

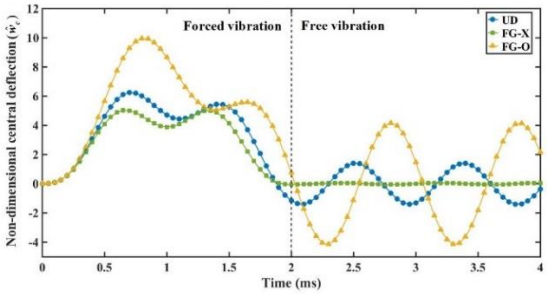

Fig. 7. Non-dimensional central deflection ($\hat{w}_c$) of the simply supported FG-CNTRC plates with various patterns subjected to the sine loading $\left(a=b=0.25\text{m},\ b/h=10,\ V^*_{CNT}=0.11\right)$.

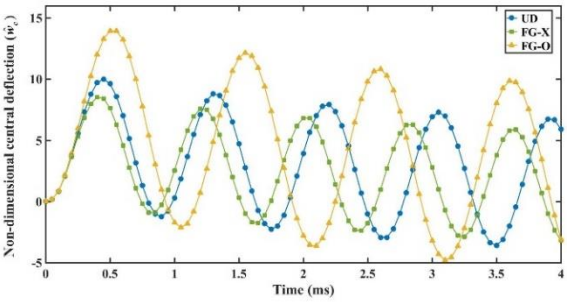

Fig. 8. Non-dimensional central deflection ($\hat{w}_c$) of the simply supported FG-CNTRC plates with various patterns subjected to

the explosive blast loading
$\left(a=b=0.25\text{m},\ b/h=10,\ V_{CNT}^{*}=0.11\right)$.

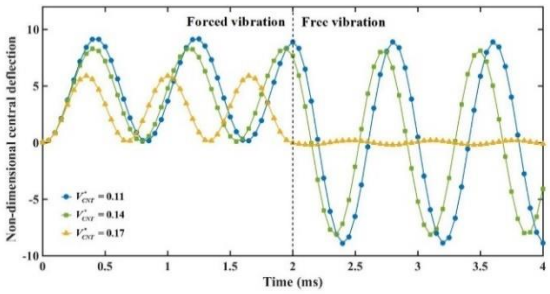

Fig. 9. Non-dimensional central deflection $(\hat{w}_c)$ of the simply supported FGX-CNTRC plates with different CNTs volume fractions subjected to the step loading
$\left(a=b=0.25\text{m},\ b/h=10\right)$.

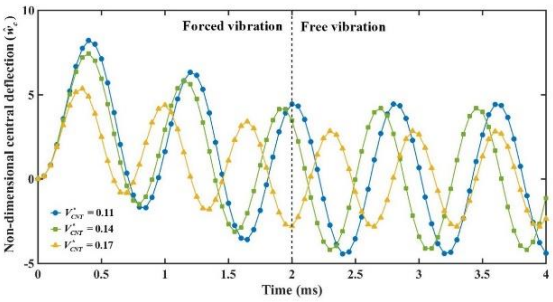

Fig. 10. Non-dimensional central deflection $(\hat{w}_c)$ of the simply supported FGX-CNTRC plates with different CNTs volume fractions subjected to the triangular loading
$\left(a=b=0.25\text{m},\ b/h=10\right)$.

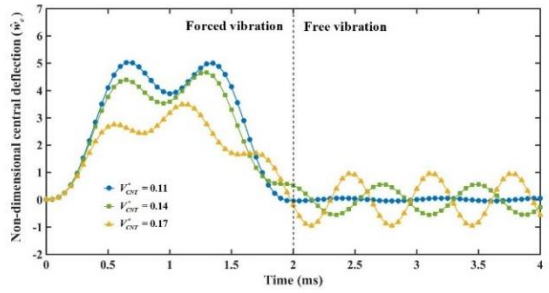

Fig. 11. Non-dimensional central deflection $(\hat{w}_c)$ of the simply supported FGX-CNTRC plates with different CNTs volume fractions subjected to the sine loading
$\left(a=b=0.25\text{m},\ b/h=10\right)$.

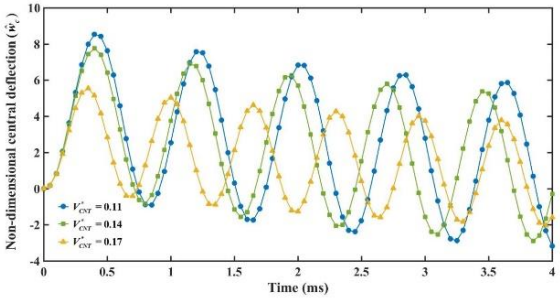

Fig. 12. Non-dimensional central deflection $(\hat{w}_c)$ of the simply supported FGX-CNTRC plates with different CNTs volume fractions subjected to the explosive blast loading
$\left(a=b=0.25\text{m},\ b/h=10\right)$.

6. Conclusion

In the present research, an efficient HSDT based isogeometric formulation is developed for free and forced vibration analyses of FG-CNTRC plates. The transverse shear deformation along the plate thickness is estimated via a logarithmic function recently proposed by Zhu et al. [38]. It is shown that in the present solution, the convergence of the results is very fast. Besides, the computed data are in very close agreement with the semi-analytical and 3D solutions. It can be concluded that the present LHSDT, when combined with the IGA, can predict very accurate natural frequencies and transient responses for FG-CNTRC plates. In addition, a detailed parametric study is executed. It is demonstrated that

- The largest values for natural frequencies of the CNTRC plates occur when the FG-X pattern is considered.
- The natural frequencies of the plate increase when more CNTs are dispersed into the polymetric matrix.
- For a certain value of CNT volume fraction, the natural frequencies of the FG-CNTRC plates decrease as the plates become thicker.
- When the plate is comparably thick, the influence of CNTs distribution on the natural frequencies of FG-CNTRC plates is very low.
- With a preassigned value for CNT volume fraction and width-to-thickness ratio, frequency parameters drop when the aspect ratio increases.
- The distribution pattern and volume fraction of CNTs have strong impacts on the dynamic response of FG-CNTRC plates.

References

[1] Iijima, S. and Ichihashi, T., 1993. Single-shell carbon nanotubes of 1-nm diameter. *Nature*, 363. pp.603-605.

[2] Liew, K.M., Lei, Z.X. and Zhang, L.W., 2015. Mechanical analysis of functionally graded carbon nanotube reinforced composites: A review. *Composite Structures*, 120, pp.90-97.

[3] Shen, H.S., 2009. Nonlinear bending of functionally graded carbon nanotube-reinforced composite plates in thermal environments. *Composite Structures*, 91, pp.9-19.

[4] Wang, Z.X. and Shen, H.S., 2011. Nonlinear vibration of nanotube-reinforced composite plates in thermal environments. *Computational Materials Science*, 50(8), pp.2319-2330.

[5] Zhu, P., Lei, Z.X. and Liew, K.M., 2012. Static and free vibration analyses of carbon nanotube-reinforced composite plates using finite element method with first order shear deformation plate theory. *Composite Structures*, 94, pp.1450-1460.

[6] Malekzadeh, P. and Shojaee, M., 2013. Buckling analysis of quadrilateral laminated plates with carbon nanotubes reinforced composite layers, Thin-Walled Structures, 71, pp.108-118.

[7] Moradi-Dastjerdi, R., Foroutan, M. and Pourasghar, A., 2013. Dynamic analysis of functionally graded nanocomposite cylinders reinforced by carbon nanotube by a mesh-free method. Materials and Design, 44, pp.256-266.

[8] Alibeigloo, A., 2014. Elasticity Solution of Functionally Graded Carbon Nanotube Reinforced Composite Cylindrical Panel. Mechanics of Advanced Composite Structures, 1, pp. 49-60.

[9] Moradi-Dastjerdi, R. and Pourasghar, A., 2014. Dynamic analysis of functionally graded nanocomposite cylinders reinforced by wavy carbon nanotube under an impact load. Journal of Vibration and Control, https://doi.org/10.1177/1077546314539368.

[10] Lei, Z.X., Zhang, L.W. and Liew, K.M., 2015. Elastodynamic analysis of carbon nanotube-reinforced functionally graded plates. International Journal of Mechanical Sciences, 99, pp.208-217.

[11] Moradi-Dastjerdi, R., Payganeh, G., RajabizadehMirakabad, S. and JafariMofrad-Taheri, M., 2016. Static and Free Vibration Analyses of Functionally Graded Nano-composite Plates Reinforced by Wavy Carbon NanotubesResting on a Pasternak Elastic Foundation. Mechanics of Advanced Composite Structures, 3, pp. 123-135.

[12] Setoodeh, A.R. and Shojaee, M., 2016. Application of TW-DQ method to nonlinear free vibration analysis of FG carbon nanotube-reinforced composite quadrilateral plates. Thin-Walled Structures, 108, pp.1-11.

[13] Moradi-Dastjerdi, R. and Payganeh, G., 2017. Thermoelastic dynamic analysis of wavy carbon nanotube reinforced cylinders under thermal loads. Steel and Composite Structures, 25, pp.315-326.

[14] Moradi-Dastjerdi, R. and Malek-Mohammadi, H., 2017. Free Vibration and Buckling Analyses of Functionally Graded Nanocomposite Plates Reinforced by Carbon Nanotube. Mechanics of Advanced Composite Structures, 4, pp. 59-73.

[15] Safaei, B., Khoda, F.H. and Fattahi, A.M., 2019. Non-classical plate model for single-layered graphene sheet for axial buckling. Advances in Nano Research, 7(4), pp.265–275.

[16] Shokri-Oojghaz, R., Moradi-Dastjerdi, R., Mohammadi, H. and Behdinan, K., 2019. Stress distributions in nanocomposite sandwich cylinders reinforced by aggregated carbon nanotube. Polymer Composites, https://doi.org/10.1002/pc.25206.

[17] Safaei, B., Moradi-Dastjerdi, R., Qin, Z. and Chu, F., 2019. Frequency-dependent forced vibration analysis of nanocomposite sandwich plate under thermo-mechanical loads. Composites Part B-Engineering, 161, pp.44-54.

[18] Xie, B., Sahmani, S., Safaei, B. and Xu, B., 2021. Nonlinear secondary resonance of FG porous silicon nanobeams under periodic hard excitations based on surface elasticity theory. Engineering with Computers, 37, pp.1611–1634.

[19] Fattahi, A.M., Safaei, B., Qin, Z., and Chu, F., 2021. Experimental studies on elastic properties of high density polyethylene-multi walled carbon nanotube nanocomposites. Steel and Composite Structures, 38, pp.177-187.

[20] Sahmani, S. and Safaei, B., 2021. Large-amplitude oscillations of composite conical nanoshells with in-plane heterogeneity including surface stress effect. Applied Mathematical Modelling, 89(2), pp.1792-1813.

[21] Moradi-Dastjerdi, R. and Behdinan, K., 2021. Free vibration response of smart sandwich plates with porous CNT-reinforced and piezoelectric layers. Applied Mathematical Modelling, 96, pp.66-79.

[22] Safaei, B. and Fattahi, A.M., 2017. Free Vibrational Response of Single-Layered

Graphene Sheets Embedded in an Elastic Matrix using Different Nonlocal Plate Models. Mechanics, 23(5), pp.678-687.

[23] Ferreira, A.J.M., Castro, L.M. and Bertoluzza, S., 2009. A high order collocation method for the static and vibration analysis of composite plates using a first-order theory. Composite Structures, 89, pp.424-432.

[24] Yin, S., Hale, J.S., Yu, T., Bui, T.Q. and Bordas, S.P.A., 2014. Isogeometric locking-free plate element: A simple first order shear deformation theory for functionally graded plates. Composite Structures, 118, pp.121-138.

[25] Yu, T., Yin, S., Hale, J.S., Bui, T.Q. and Hirose, S., 2015. A simple FSDT-based isogeometric analysis for geometrically nonlinear analysis of functionally graded plates. Finite Elements in Analysis and Design, 96, pp.1-10.

[26] Thai, C.H., Zenkour, A.M., Abdel-Wahab, M. and Nguyen-Xuan, H., 2016. A simple four-unknown shear and normal deformations theory for functionally graded isotropic and sandwich plates based on isogeometric analysis. Composite Structures, 139, pp.77-95.

[27] Reddy, J.N., 1984. A simple higher-order theory for laminated composite plates. Journal of Applied Mechanics, 51(4), pp.745-752.

[28] Xiang, S., Jin, Y.X., Bi, Z.Y., Jiang, S.X. and Yang, M.S., 2011. A n-order shear deformation theory for free vibration of functionally graded and composite sandwich plates. Composite Structures, 93, pp.2826-2832.

[29] Darijani, H. and Shahdadi, A.H., 2015. A new shear deformation model with modified couple stress theory for microplates. Acta Mechanica, 226, pp.2773-2788.

[30] Nguyen, N.T., Hui, D., Lee, J. and Nguyen-Xuan, H., 2015. An efficient computational approach for size-dependent analysis of functionally graded nanoplates. Computer Methods in Applied Mechanics and Engineering, 297, pp.191-218.

[31] Touratier, M., 1991. An efficient standard plate theory. International Journal of Engineering Science, 29(8), pp.901-916.

[32] Mantari, J.L., Oktem, A.S. ans Soares, C.G., 2012. A new trigonometric shear deformation theory for isotropic, laminated and sandwich plates. International Journal of Solids and Structures, 49, pp.43-53.

[33] Soldatos, K.P., 1992. A transverse shear deformation theory for homogeneous monoclinic plates. Acta Mechanica, 94(3) pp.195-220.

[34] Mahi, A., Adda Bedia, E.A. and Tounsi, A., 2015. A new hyperbolic shear deformation theory for bending and free vibration analysis of isotropic, functionally graded, sandwich and laminated composite plates. Applied Mathematical Modelling, 39(9), pp.2489-2508.

[35] Karama, M., Afaq, K.S. and Mistou, S., 2003. Mechanical behaviour of laminated composite beam by the new multi-layered laminated composite structures model with transverse shear stress continuity. International Journal of Solids and Structures, 40(6), pp.1525-1546.

[36] Aydogdu, M., 2009. A new shear deformation theory for laminated composite plates. Composite Structures, 89(1) pp.94-101.

[37] Mantari, J.L., Oktem, A.S. and Soares, C.G., 2012. A new higher order shear deformation theory for sandwich and composite laminated plates. Composites Part B-Engineering, 43(3) pp.1489-1499.

[38] Zhu, Y., Shi, P., Kang, Y. and Cheng, B., 2019. Isogeometric analysis of functionally graded plates with a logarithmic higher order shear deformation theory. Thin-Walled Structures, 144, pp.106234.

[39] Hughes, T.J.R., Cottrell, J.A. and Bazilevs, Y., 2005. Isogeometric analysis: CAD, finite elements, NURBS, exact geometry and mesh refinement. Computer Methods in Applied Mechanics and Engineering, 194, pp.4135-4195.

[40] Shojaee, S., Valizadeh, N., Izadpanah, E., Bui, T. and Vu, T.V., 2012. Free vibration and buckling analysis of laminated composite plates using the NURBS-based isogeometric finite element method. Composite Structures, 94(5), pp.1677-1693.

[41] Benson, D.J., Bazilevs, Y., Hsu, M.C. and Hughes, T.J.R., 2010. Isogeometric shell analysis: The Reissner–Mindlin shell. Computer Methods in Applied Mechanics and Engineering, 199, pp.276-289.

[42] Thai, C.H., Nguyen-Xuan, H., Nguyen-Thanh N., Le, T.H., Nguyen-Thoi, T. and Rabczuk, T., 2012. Static, free vibration, and buckling analysis of laminated composite Reissner–Mindlin plates using NURBS-based isogeometric approach. International Journal for Numerical Methods in Engineering, 91(6), pp.571-603.

[43] Yu, T., Bui, T.Q., Yin, S., Wu, C.T., Do, T.V. and Tanaka, S., 2016. On the thermal buckling analysis of functionally graded plates with internal defects using extended isogeometric analysis. Composite Structures, 136, pp.684-695.

[44] Abdollahzadeh Shahrbabaki, E. and Alibeigloo, A., 2014. Three-dimensional free vibration of carbon nanotube-reinforced composite plates with various boundary conditions using Ritz method, Composite Structures, 111, pp.362-372.

[45] Zhang, L.W., Song, Z.G. and Liew, K.M., 2015. State-space Levy method for vibration analysis of FG-CNT composite plates subjected to in-plane loads based on higher-order shear deformation theory. Composite Structures, 134, pp.989-1003.

[46] Duc, N.D., Lee, J., Nguyen-Thoi, T. and Thang, P.T., 2017. Static response and free vibration of functionally graded carbon nanotube-reinforced composite rectangular plates resting on Winkler-Pasternak elastic foundations. Aerospace Science and Technology, 68, pp.391-402.

[47] Malekzadeh, P. and Heydarpour, Y., 2015. Mixed Navier-layerwise differential quadrature threedimensional static and free vibration analysis of functionally graded carbon nanotube reinforced composite laminated plates. Meccanica, 50, pp.143-167.

[48] Alibeigloo, A. and Emtehani, A., 2015. Static and free vibration analyses of carbon nanotube reinforced composite plate using differential quadrature method. Meccanica, 50, pp.61-76.

[49] Wang, M., Li, Z.M. and Qiao, P., 2016. Semi-analytical solutions to buckling and free vibration analysis of carbon nanotube-reinforced composite thin plates. Composite Structures, 144, pp.33-43.

[50] Lei, Z.X., Liew, K.M. and Yu, J.L., 2013. Free vibration analysis of functionally graded carbon nanotube-reinforced composite plates using the element-free kp-Ritz method in thermal environment. Composite Structures, 106, pp.128-138.

[51] Wu, C.P. and Li, H.Y., 2014. Three-dimensional free vibration analysis of functionally graded carbon nanotube-reinforced composite plates with various boundary conditions. Journal of Vibration and Control, https://doi.org/10.1177/1077546314528367.

[52] Malekzadeh, P. and Zarei, A.R., 2014. Free vibration of quadrilateral laminated plates with carbon nanotube reinforced composite layers. Thin-Walled Structures, 82, pp.221-232.

[53] Zhang, L.W., Lei, Z.X. and Liew, K.M., 2015. Free vibration analysis of functionally graded carbon nanotube-reinforced composite triangular plates using the FSDT and element-free IMLS-Ritz method. Composite Structures, 120, pp.189-199.

[54] Zhang, L.W., Cui, W.C. and Liew, K.M., 2015. Vibration analysis of functionally graded carbon nanotube reinforced composite thick plates with elastically restrained edges. International Journal of Mechanical Sciences, 134, pp.9-21.

[55] Zhang, L.W., Lei, Z.X. and Liew, K.M., 2015. Vibration characteristic of moderately thick functionally graded carbon nanotube reinforced composite skew plates, Composite Structures. 122, pp.172-183.

[56] Mehar, K., Panda, S.K., Dehengia, A. and Kar, V.R., 2015. Vibration analysis of functionally graded carbon nanotube reinforced composite plate in thermal environment. Journal of Sandwich Structures and Materials, https://doi.org/10.1177/1099636215613324.

[57] Phung-Van, P., Abdel-Wahab, M., Liew, K.M., Bordas, S.P.A. and Nguyen-Xuan, H., 2015. Isogeometric analysis of functionally graded carbon nanotube-reinforced composite plates using higher-order shear deformation theory. Composite Structures, 123, pp.137-149.

[58] Garcia-Macias, E., Castro-Triguero, R., Flores, E.I.S., Friswell, M.I. and Gallego, R., 2016. Static and free vibration analysis of functionally graded carbon nanotube reinforced skew plates. Composite Structures, 140, pp.473-490.

[59] Kiani, Y., 2016. Free vibration of FG-CNT reinforced composite skew plates. Aerospace Science and Technology, 58, pp.178-188.

[60] Ansari, R., Torabi, J. and Hassani R., 2019. A comprehensive study on the free vibration of arbitrary shaped thick functionally graded CNT-reinforced composite plates. Engineering Structures, 181, pp.653-669.

[61] Majidi, M.H., Azadi, M. and Fahham H., 2020. Vibration analysis of cantilever FG-CNTRC trapezoidal plates, Journal of the Brazilian Society of Mechanical Sciences and Engineering. https://doi.org/10.1007/s40430-019-2151-7.

[62] Mohammadi, H. and Setoodeh, A.R., 2020. Free vibration analysis of functionally graded carbon nanotubes reinforced composite skew folded plates using isogeometric approach. Amirkabir Journal of Mechanical Engineering, doi: 10.22060/mej.2020.17298.6569.

[63] Qin, Z., Pang, X., Safaei, B. and Chu, F., 2019. Free vibration analysis of rotating functionally graded CNT reinforced composite cylindrical shells with arbitrary boundary conditions. Composite Structures, 220, pp. 847-860.

[64] Thai, C.H., Kulasegaram, S., Tran, L.V. and Nguyen-Xuan, H., 2014. Generalized shear deformation theory for functionally graded isotropic and sandwich plates based on isogeometric approach. Computers and Structures, 141, pp.94-112.

[65] Tran, L.V., Ly, H.A., Lee, J., Abdel-Wahab, M. and Nguyen-Xuan, H., 2015. Vibration analysis of cracked FGM plates using higher-order shear deformation theory and extended isogeometric approach. International Journal of Mechanical Sciences, 96-97, pp.65-78.

[66] Moradi-Dastjerdi, R., Radhi, A. and Behdinan, K., 2020. Damped dynamic behavior of an advanced piezoelectric sandwich plate. Composite Structures, 243, pp. 112243.

[67] Moradi-Dastjerdi, R. and Behdinan, K., 2020. Temperature effect on free vibration response of a smart multifunctional sandwich plate. Journal of Sandwich Structures and Materials, https://doi.org/10.1177/1099636220908707.

[68] Moradi-Dastjerdi, R. and Behdinan, K., 2021. Stress waves in thick porous graphene-reinforced cylinders under thermal gradient environments. Aerospace Science and Technology, 110, pp. 106476.

[69] Qao, W., Qin, Z. and Chu, F., 2020. Wave propagation in functionally graded porous plates reinforced with graphene platelets. Aerospace Science and Technology, 102, pp. 105860.

[70] Qin, Z., Zhao, S., Pang, X., Safaei, B. and Chu, F., 2020. A unified solution for vibration analysis of laminated functionally graded shallow shells reinforced by graphene with general boundary conditions. International Journal of Mechanical Sciences, 170, pp.105341.

[71] Safaei, B., 2020. The effect of embedding a porous core on the free vibration behavior of laminated composite plates. Steel and Composite Structures, 35(5), pp.659-670.

[72] Piegl, L. and Tiller, W., 1997. The NURBS book (monographs in visual communication). 2nd edn. Springer, New York.

[73] Fan, F., Xu, Y., Sahmani, S. and Safaei, B., 2020. Modified couple stress-based geometrically nonlinear oscillations of porous functionally graded microplates using NURBS-based isogeometric approach. Computer Methods in Applied Mechanics and Engineering, 372, pp. 113400.

[74] Mohammadi, H. and Setoodeh, A.R., 2019. FSDT-Based Isogeometric Analysis for Free Vibration Behavior of Functionally Graded Skew Folded Plates. Iranian Journal of Science and Technology, Transactions of Mechanical Engineering, https://doi.org/10.1007/s40997-019-00320-0.

[75] Kiani, Y., 2017. Dynamics of FG-CNT reinforced composite cylindrical panel subjected to moving load. Thin-Walled Structures, 111, pp.48-57.

[76] Reddy, J.N., 2004. An Introduction to Nonlinear Finite Element Analysis. Oxford University Press.

[77] Maleki, S., Tahani, M. and Andakhshideh, A., 2012. Transient response of laminated plates with arbitrary laminations and boundary conditions under general dynamic loadings. Archive of Applied Mechanics, 82, pp.615-630.